Desalination and Water Treatment 324 (2025) 101558

Contents lists available at ScienceDirect

Desalination and Water Treatment

journal homepage: www.sciencedirect.com/journal/desalination-and-water-treatment/

PVC microplastics as vectors for dye pollutants: Adsorption of rhodamine B and AI-based predictive modeling

Vinícius Reis Cargnelutti [a], Rossean Golin [b], Amanda Alcaide Francisco Fukumoto [b], Ibraim Fantin da Cruz [b], Frederico Carlos Martins de Menezes Filho [c], Paulo Renato Matos Lopes [d], Rodrigo Esaú Vassoler e Silva [e], Leonardo Gomes de Vasconcelos [e], Danila Soares Caixeta [b], Eduardo Beraldo de Morais [b,*]

[a] Faculty of Engineering, Federal University of Mato Grosso, Várzea Grande, MT, Brazil
[b] Department of Sanitary and Environmental Engineering, Federal University of Mato Grosso, Cuiabá, MT, Brazil
[c] Institute of Exact and Technological Sciences, Federal University of Viçosa, Rio Paranaíba, MG, Brazil
[d] Department of Plant Production, College of Agricultural and Technological Sciences, São Paulo State University, Dracena, SP, Brazil
[e] Department of Chemistry, Federal University of Mato Grosso, Cuiabá, MT, Brazil

ARTICLE INFO

Keywords:
ANN
SVR
Adsorption mechanisms
Polyvinyl chloride microplastics
Artificial intelligence

ABSTRACT

Microplastics are persistent pollutants in aquatic ecosystems and can act as carriers of contaminants. Understanding how these particles adsorb and transport contaminants is crucial for assessing their ecological risks. In this study, the adsorption of Rhodamine B (RhB) onto polyvinyl chloride microplastics (PVC-MPs) was evaluated under varying pH, dye concentration, microplastic dosage, and contact time. PVC-MPs exhibited a specific surface area of 0.1713 $m^2\ g^{-1}$ and pore volume of 0.0010 $cm^3\ g^{-1}$, consistent with a compact structure. Despite this, they achieved a maximum adsorption capacity of 2.09 mg g^{-1}, with higher uptake under acidic conditions. Kinetic analysis showed that the pseudo-first-order model provided the best fit ($R^2 > 0.980$), while equilibrium data were best represented by the Temkin ($R^2 = 0.967$) and Dubinin–Radushkevich ($R^2 = 0.968$) models. The low mean adsorption energy (E = 0.0937 kJ mol^{-1}) confirmed that physisorption dominated the process. FTIR spectra indicated weak interactions such as hydrophobic forces, hydrogen and halogen bonding, and van der Waals forces. Artificial intelligence models showed excellent predictive performance on the test set: ANN achieved $R^2 = 0.999$ and RMSE = 0.0142, while SVR reached $R^2 = 0.992$ and RMSE = 0.0354. Overall, these findings highlight the environmental relevance of PVC-MPs as vectors of synthetic dyes, emphasizing their potential risks to ecosystems and human health and the need for ecotoxicological evaluations.

1. Introduction

Plastics have become indispensable materials in modern society due to their versatility, mechanical strength, and relatively low production costs. Their lightweight nature and resistance to corrosion, chemical agents, and physical degradation have supported their widespread application in diverse fields such as packaging, construction, transportation, electronics, and consumer products [1,2]. However, the extensive use of plastics, coupled with inefficient waste management, has resulted in the accumulation of plastic residues in natural environments. Among these, microplastics (MPs, typically defined as particles between 0.1 and 5 mm) are now recognized as pervasive pollutants in both aquatic and terrestrial systems [3]. Their persistence and wide distribution have raised increasing concern due to their potential ecological impacts, including bioaccumulation, trophic transfer, and altered organismal physiology in aquatic species, as well as possible human health risks through ingestion, inhalation, and exposure to associated contaminants [4–11]. These concerns have motivated extensive investigations into the environmental dynamics, interactions, and risks associated with MPs.

Microplastics encompass a wide range of polymeric materials, including polyvinyl chloride, polystyrene, polyethylene, polypropylene,

* Corresponding author.
E-mail address: eduardo.morais@ufmt.br (E.B. de Morais).

https://doi.org/10.1016/j.dwt.2025.101558
Received 30 August 2025; Received in revised form 5 November 2025; Accepted 6 November 2025
Available online 7 November 2025
1944-3986/© 2025 The Author(s). Published by Elsevier Inc. This is an open access article under the CC BY-NC-ND license (http://creativecommons.org/licenses/by-nc-nd/4.0/).

and polyester, and are commonly categorized into two main groups: primary and secondary [12,13]. Primary microplastics are deliberately manufactured at small sizes for specific applications, such as microbeads in cosmetics, industrial resin pellets, and synthetic textile fibers. Secondary microplastics, in contrast, originate from the breakdown of larger plastic items, a process accelerated by environmental stressors such as ultraviolet radiation, temperature variation, and physical abrasion [2,14]. Among these polymers, PVC is widely used in pipes, packaging, flooring, and medical devices, and its environmental degradation through physical, chemical, and biological weathering leads to the formation of persistent secondary PVC microplastics. Its hydrophobic surface, chlorine content, and smooth texture make it highly resistant to degradation, contributing to its long-term persistence in aquatic environments [15].

The relatively high surface area-to-volume ratio of MPs contributes to their strong capacity for binding anthropogenic pollutants, enabling them to act as carriers that facilitate contaminant transport across ecosystems and trophic levels [13,14]. Because of the inherent hydrophobicity of their polymeric surfaces, MPs tend to accumulate nonpolar compounds [16]. Weathering processes, such as photooxidation and mechanical abrasion, can further introduce oxygen-containing functional groups, thereby increasing their affinity for polar substances [17]. Consequently, a broad spectrum of pollutants has been shown to associate with MPs, including persistent hydrophobic contaminants such as polychlorinated biphenyls (PCBs) [18], pesticides [19], and polycyclic aromatic hydrocarbons [20], as well as more polar emerging contaminants such as pharmaceuticals, antibiotics, and personal care products [21–23]. These interactions are governed by multiple mechanisms, including hydrophobic interactions, van der Waals forces, hydrogen bonding, and electrostatic attractions, which can act synergistically depending on polymer type and environmental conditions [15,24]. Once adsorbed, pollutants can be transported over long distances or become more bioavailable to aquatic organisms, potentially leading to bioaccumulation, trophic transfer, and enhanced ecotoxicological risks in aquatic systems [10,25].

Synthetic dyes are recognized as a significant group of environmental contaminants because of their chemical stability, toxic potential, and detrimental impacts on aquatic ecosystems [26–31]. When adsorbed onto MPs, these compounds may exhibit increased persistence and bioavailability, thereby intensifying their ecological risks [32]. Several recent studies have investigated the interaction between MPs and dyes, revealing that these materials can exhibit measurable adsorption capacities and influence contaminant transport. For instance, Bahrami et al. [33] showed that polyethylene microplastics are capable of adsorbing methylene blue from water, while Nasrabadi et al. [10] reported significant adsorption of crystal violet onto polystyrene microplastics, demonstrating their ability to retain synthetic dyes under various conditions. Despite these advances, relatively few studies have examined the adsorption behavior of hydrophilic dyes on MPs under environmentally relevant conditions, leaving key aspects of their role as pollutant carriers unresolved. A deeper understanding of MP–dye interactions is therefore crucial for evaluating the environmental fate of these substances and for guiding the development of effective mitigation strategies.

The interaction of contaminants with MPs is governed by multiple environmental and material-dependent factors, such as pH, temperature, contaminant concentration, salinity, and the intrinsic physical and chemical features of the polymers [12,32]. Properties including surface roughness, hydrophobicity, and polymer type are particularly influential in defining the adsorption potential of MPs [14]. Experimental investigations of these influencing factors are often labor-intensive and costly. To address these challenges, artificial intelligence (AI) techniques, particularly artificial neural networks (ANN) and support vector regression (SVR), have emerged as powerful tools for modeling and predicting adsorption behavior by capturing complex relationships among environmental variables [34]. These models have been successfully applied to predict dye adsorption onto a variety of adsorbents, including activated carbon, biochar, and plant-based materials [35–37]. However, the application of AI-based modeling to assess dye adsorption onto MPs remains underexplored. Leveraging such techniques may not only streamline the modeling of adsorption dynamics but also offer deeper mechanistic insights, contributing to more effective strategies for mitigating the environmental risks associated with MP contamination.

This study investigates the adsorption of Rhodamine B (RhB) onto polyvinyl chloride microplastics (PVC-MPs) to clarify their role as carriers of organic dyes in aquatic environments. PVC is one of the most widely produced plastics, and its residues are frequently detected in water systems, while RhB is a persistent and potentially toxic xanthene dye commonly used in textiles, printing, and microscopy [34]. The study combines controlled adsorption experiments—evaluating the effects of pH, particle dosage, and dye concentration—with artificial intelligence models (ANN and SVR) to predict adsorption behavior. This integrative approach addresses a critical knowledge gap regarding dye–microplastic interactions and contributes to a broader understanding of the environmental risks associated with MPs as pollutant vectors.

2. Materials and methods

2.1. Materials

RhB (molecular formula: $C_{28}H_{31}ClN_2O_3$; molecular weight: 479.01 g mol^{-1}) was obtained from Synth (Brazil). A stock solution of 500 mg L^{-1} was prepared in distilled water and further diluted to the concentrations required for the experiments. Sodium hydroxide (NaOH), hydrochloric acid (HCl), and potassium nitrate (KNO_3), all analytical grade, were also purchased from Synth (Brazil). Solution pH adjustments were carried out with 0.1 M NaOH or 0.1 M HCl, depending on the target condition.

Polyvinyl chloride microplastics (PVC-MPs) were produced from post-consumer PVC residues provided by a local recycling facility in Brazil. The material was first rinsed thoroughly with distilled water, dried at room temperature, and subsequently ground in a high-speed crusher. The resulting particles were sieved through a 63 μm mesh, and the fraction below this size was collected for use in adsorption assays, as this cutoff ensures smaller particles with higher surface area-to-volume ratios and follows common practice in MP studies [38,39].

2.2. PVC-MPs characterization

The physical and chemical features of the PVC-MPs were investigated using a set of complementary analytical techniques. Surface morphology and elemental composition were examined by scanning electron microscopy (SEM, Jeol JSM-IT 300) operated at an accelerating voltage of 15 kV, coupled with energy-dispersive X-ray spectroscopy (EDS, Balzers Union MED 010). Functional groups were assessed by Fourier-transform infrared spectroscopy (FTIR, Shimadzu IRAffinity-1) using the KBr pellet method, in the spectral region from 4000 to 400 cm^{-1}. Crystallinity was evaluated through X-ray diffraction (XRD, Bruker D8 Advance) using Cu Kα radiation operated at 40 kV and 40 mA. Diffraction patterns were collected over a 2θ range of 5–80°, with a step size of 0.02°, an acquisition time of 0.5 s per step, and a divergence slit of 0.2 mm. Textural characteristics, including surface area, pore size distribution, and pore volume, were obtained with a Micromeritics TriStar II PLUS system. The Brunauer–Emmett–Teller (BET) method was applied for specific surface area determination, whereas pore size and volume were estimated using the Barrett–Joyner–Halenda (BJH) approach from nitrogen adsorption–desorption isotherms at 77 K. The point of zero charge (pH_{PZC}) was determined using the batch equilibrium technique with 0.1 M KNO_3 solutions at different initial pH values, adjusted with either 0.1 M NaOH or 0.1 M HCl. For each measurement, 0.03 g of PVC-MPs was dispersed in 25 mL of solution and agitated at 24

°C for 24 h. The pH_{PZC} was identified from the intersection point of the curve plotting ΔpH (final pH − initial pH) against the initial pH.

2.3. Batch adsorption experiments

Batch adsorption assays were carried out in 100 mL Erlenmeyer flasks, each containing 40 mL of RhB solution. The suspensions were kept under agitation at 180 rpm in a temperature-controlled orbital shaker set to 25 °C. To evaluate the adsorption process, the influence of several parameters was examined: initial pH (2, 4, 6, 8, and 10), PVC-MP dosage (50–400 mg), initial dye concentration (10–75 mg L^{-1}), and contact time (1–24 h). All tests were performed in triplicate to ensure experimental reliability. Following adsorption, the suspensions were passed through 0.45 μm membrane filters, and the remaining RhB concentration in solution was measured with a UV–Vis spectrophotometer (Hach DR6000) at 552 nm. Quantification was based on a calibration curve (Figure S1) The adsorption capacity of PVC-MPs at time t (q_t, mg g^{-1}) was obtained according to Equation (1):

$$q_t = \frac{(C_0 - C_t) \quad V}{m} \tag{1}$$

where C_0 (mg L^{-1}) is the initial RhB concentration, C_t (mg L^{-1}) is the concentration at time t, V (L) is the solution volume, and m (g) is the mass of PVC-MPs used.

2.4. Kinetic and equilibrium studies

Kinetic experiments were performed at initial RhB concentrations of 10, 20, and 50 mg L^{-1} using 40 mL of solution in 100 mL Erlenmeyer flasks, agitated at 180 rpm and 25 °C. Assays were conducted at the natural pH (5.5) with a fixed PVC-MP dosage of 100 mg (solid–liquid ratio = 2.5 g L^{-1}), with contact times ranging from 1 to 24 h. All runs were performed in triplicate. To interpret the adsorption dynamics, three kinetic models commonly applied in adsorption studies were considered: pseudo-first-order (PFO), pseudo-second-order (PSO), and intraparticle diffusion [40].

The PFO model is given by:

$$q_t = \quad q_e(1 - e^{-K_1 t}) \tag{2}$$

The PSO model is described as:

$$q_t = \frac{K_2 {q_e}^2 t}{1 + K_2 q_e t} \tag{3}$$

The intraparticle diffusion model is represented by:

$$q_t = K_{id} t^{1/2} + C \tag{4}$$

In these expressions, q_e and q_t (mg g^{-1}) denote the adsorption capacities of RhB at equilibrium and at time t (h), respectively. K_1 (h^{-1}) and K_2 (g mg^{-1} h^{-1}) correspond to the rate constants of the PFO and PSO models, respectively. K_{id} (mg g^{-1} $min^{-0.5}$) represents the intraparticle diffusion rate constant, while C (mg g^{-1}) is the intercept, associated with the influence of the boundary layer.

Equilibrium adsorption experiments were conducted using 40 mL of RhB solution at initial concentrations ranging from 10 to 75 mg L^{-1}, with 100 mg of PVC-MPs at the natural pH (5.5) and 25 °C, under agitation at 180 rpm. The equilibrium data were fitted to four classical adsorption isotherm models, Langmuir, Freundlich, Temkin, and Dubinin–Radushkevich (D–R), as shown in Equations (5) to (8) [41,42].

The Langmuir isotherm can be represented as:

$$q_e = \quad \frac{q_{max} K_L C_e}{1 + K_L C_e} \tag{5}$$

The Freundlich isotherm is formulated as:

$$q_e = \quad K_F {C_e}^{1/n} \tag{6}$$

The Temkin isotherm is expressed as:

$$q_e = \quad \frac{RT}{b_T} \ln A_T C_e \tag{7}$$

The D–R isotherm is written as:

$$q_e = \quad q_{max} e^{-\beta \varepsilon^2}; \varepsilon = RT \; ln\left(1 + \quad \frac{1}{C_e}\right) \tag{8}$$

In these equations, q_e (mg g^{-1}) denotes the equilibrium adsorption capacity, while C_e (mg L^{-1}) is the RhB concentration at equilibrium. q_{max} (mg g^{-1}) and K_L (L mg^{-1}) are the Langmuir parameters, describing the maximum adsorption capacity and the affinity of the adsorbent sites, respectively. K_f ((mg g^{-1})(mg $L^{-1})^{-1/n}$) and n are the Freundlich constants associated with adsorption capacity and heterogeneity. A_T (L g^{-1}) and b_T (J mol^{-1}) are the Temkin constants, related to the binding constant and the heat of adsorption. For the D–R model, β (mol^2 J^{-2}) is the energy constant and ε represents the Polanyi potential. R (8.314 J mol^{-1} K^{-1}) is the universal gas constant, and T (K) is the absolute temperature.

2.5. ANN and SVR modeling

Artificial neural networks (ANNs) were used to predict the adsorption of RhB onto PVC-MPs. The ANN model consisted of three layers (input, hidden, and output). Each neuron in the hidden layer applied an activation function to capture nonlinear relationships among variables, while the backpropagation algorithm iteratively adjusted weights and biases to minimize prediction errors [35,37]. Several activation functions, such as sigmoid, hyperbolic tangent (tanh), and exponential, were tested, and the configuration yielding the best performance on the test set was selected [43]. A detailed description of the ANN model and a schematic representation of its architecture are provided in the Supplementary Material (Text S1, Figure S2).

Support vector regression (SVR) was also employed to model the adsorption capacity. In this method, a regression function is constructed within an ε-insensitive margin, where deviations smaller than ε are disregarded, and only errors outside this region contribute to the optimization [44]. The predictive performance depends mainly on three factors: the penalty parameter (C), which balances model complexity and error tolerance, the ε value, which defines the margin width, and the kernel function, which maps the input data into higher-dimensional spaces [45,46]. In this study, the radial basis function (RBF) kernel was selected due to its effectiveness in capturing nonlinear patterns in adsorption processes [44]. A detailed description of the SVR model and a schematic illustration of its framework are provided in the Supplementary Material (Text S1, Figure S3).

For both approaches, four input variables (pH, dye concentration, PVC-MP dosage, and contact time) were considered, and adsorption capacity (q, mg g^{-1}) was defined as the output. Modeling was performed using TIBCO Statistica 14.0 (TIBCO Software Inc.). The dataset was randomly split into training (70 %) and test (30 %) subsets to allow independent performance assessment. Prior to training, all input variables were normalized to a 0–1 range to ensure comparability and prevent scale bias.

2.6. Model performance evaluation

The accuracy of the kinetic, equilibrium, and machine learning models (ANN and SVR) was assessed using two statistical indicators: the coefficient of determination (R^2) and the root mean squared error (RMSE). These metrics quantify the agreement between experimental and predicted adsorption capacities, allowing for a consistent comparison of model performance. The equations used for calculating R^2 and RMSE are provided in the Supplementary Material (Equations S1 and S2). Higher R^2 values and lower RMSE values indicate better model performance.

3. Results and discussion

3.1. Characteristics of PVC-MPs

The SEM micrographs of PVC-MPs are presented in Figs. 1a and 1b. The images reveal that the PVC microplastics exhibit irregular shapes and a wide range of particle sizes. The surface morphology shows a rough texture with prominent folds and creases, which may enhance the available surface area for contaminant adsorption. Elemental analysis (Fig. 1c) confirmed that the PVC-MPs are primarily composed of carbon, chlorine, oxygen, and calcium. The presence of carbon and chlorine is consistent with the chemical structure of polyvinyl chloride (PVC), while oxygen and calcium likely originate from surface oxidation processes or residual additives and impurities introduced during manufacturing or environmental degradation [47].

The point of zero charge (pH_{PZC}) of the PVC-MPs was found to be 9.67 (Figure S4). Accordingly, the particle surface acquires a positive charge at solution pH values below this threshold and becomes negatively charged at higher pH levels. This behavior directly influences the electrostatic interactions established between PVC-MPs and ionic species during adsorption.

Fig. 2 shows the FTIR spectra of PVC-MPs before and after exposure to RhB. The spectrum obtained for pristine PVC-MPs displays several characteristic absorptions. A broad band at 3448 cm^{-1} is associated with O–H stretching, which may arise from residual surface moisture or oxidative processes. Signals at 2916 and 2854 cm^{-1} correspond to C–H stretching in $–CH_2$ groups along the polymer backbone [48]. The absorption near 1689 cm^{-1} is indicative of carbonyl (C═O) groups, providing evidence of surface oxidation [49]. Additional peaks at 1427

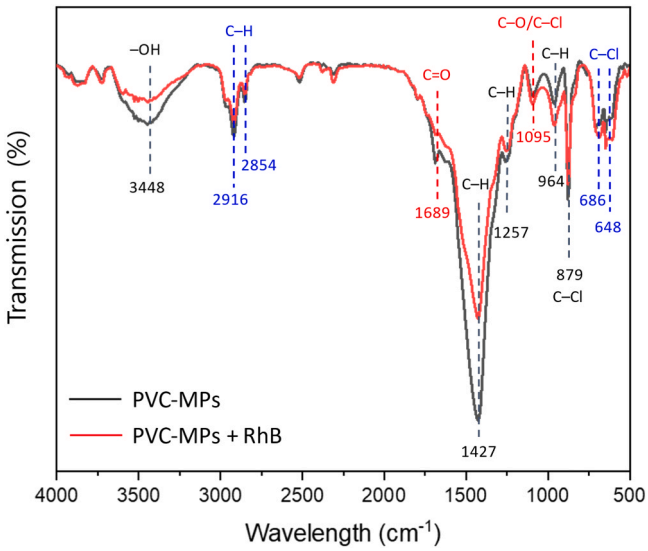


Fig. 2. FTIR spectra of PVC-MPs before and after RhB adsorption.

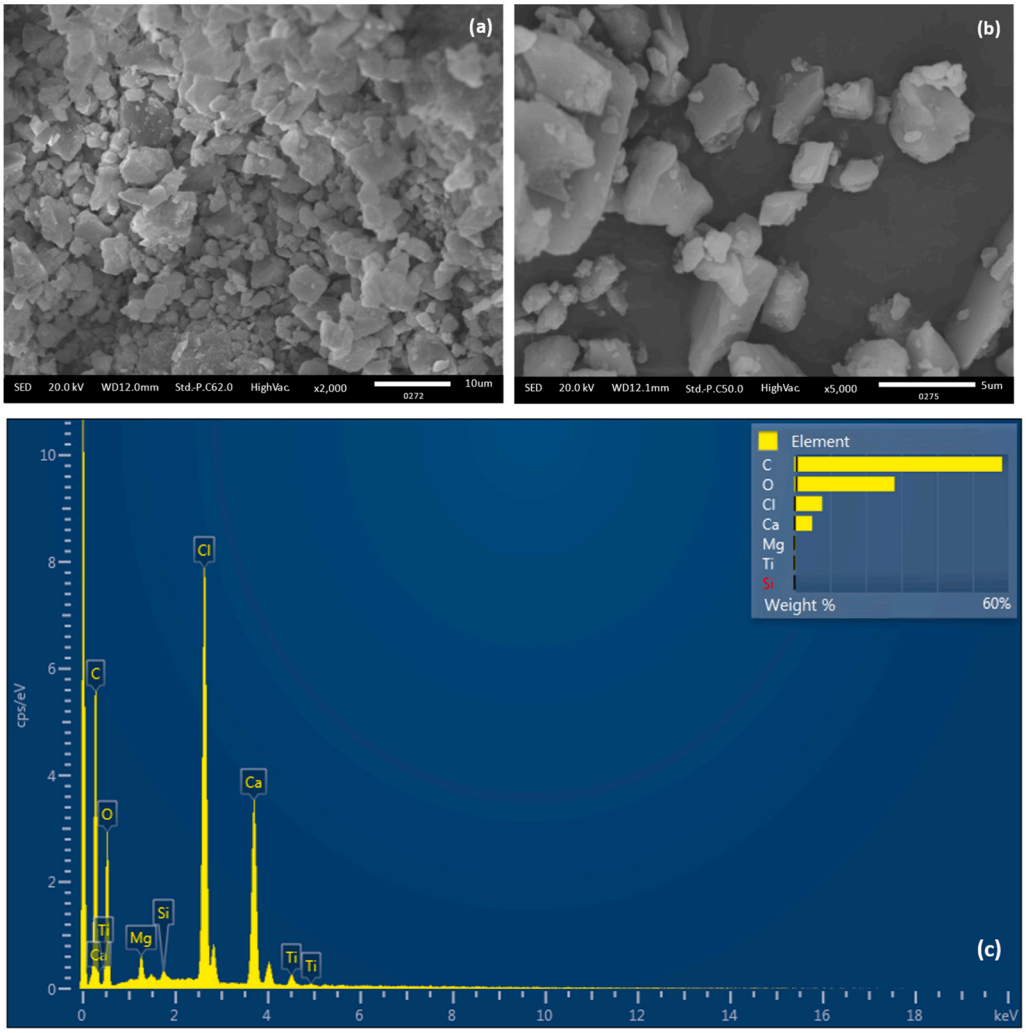


Fig. 1. SEM micrographs of PVC-MPs at (a) × 2000 and (b) × 5000 magnification, and (c) EDS spectrum showing their elemental composition.

and 1257 cm^{-1} can be ascribed to C–H bending and wagging modes in the vinyl groups, while the band at 1095 cm^{-1} reflects C–O or C–Cl stretching. Features at 964 and 879 cm^{-1} are linked to C–H deformation and C–Cl stretching vibrations, both typical of the PVC structure [47, 50]. Further confirmation of the polymer identity is given by the bands at 686 and 648 cm^{-1}, which also correspond to C–Cl stretching [1]. Overall, these assignments are consistent with those previously reported for PVC [41].

After RhB adsorption, the spectra did not display marked shifts in band positions, suggesting that no new covalent bonds were formed, i.e., chemisorption did not occur [1]. Nonetheless, a reduction in intensity was noted at 3448, 1427, 686, and 648 cm^{-1}, which can be interpreted as evidence of weak physical interactions, likely hydrogen bonding and halogen bonding, between dye molecules and the PVC-MP surface [1, 17].

The XRD pattern exhibited distinct diffraction peaks at 23.10°, 29.47°, 36.05°, 39.49°, 41.15°, 43.23°, 47.20°, and 48.59° (2θ) (Fig. 3), which correspond to the crystallographic planes of calcite ($CaCO_3$), as referenced in ICDD PDF #96–901–6707. The most intense peak at 29.47° is assigned to the (104) plane, the principal reflection of calcite. The presence of these characteristic reflections confirms calcite as the main crystalline phase in the PVC-MPs, likely resulting from the use of calcium carbonate as a mineral filler during production. The findings agree with those of Meng et al. [47], who reported calcite as the main crystalline phase in commercial PVC microplastics.

Textural characterization of the PVC-MPs showed a very low specific surface area (0.1713 m^2 g^{-1}) as obtained from the BET method. According to BJH analysis, the material exhibited a pore volume of 0.0010 cm^3 g^{-1} and an average pore diameter of 8.018 nm. These measurements reflect the compact structure and limited porosity that are typical of microplastics [33]. Comparable values were reported by Bao et al. [41] for PVC-based MPs.

3.2. Effect of pH on adsorption

The influence of pH on RhB adsorption by PVC-MPs was evaluated over a pH range from 2 to 10 (Fig. 4). Maximum adsorption was observed under acidic conditions, with capacities of 0.286, 0.272, and 0.249 mg g^{-1} at pH 2, 4, and 6, respectively. As the pH increased, the adsorption efficiency dropped markedly, reaching only 0.126 mg g^{-1} at pH 8 and 0.039 mg g^{-1} at pH 10. These results indicate that PVC-MPs exhibit greater RhB adsorption under acidic conditions, in agreement with previous studies reporting enhanced RhB uptake by MPs at low pH [50].

At pH values below 3.7, which corresponds to the pKa of RhB, the dye exists predominantly in its cationic form [50]. Although the PVC-MP surface is also positively charged under these conditions ($pH < pH_{PZC}$), the expected electrostatic repulsion did not prevent adsorption to a significant extent. This behavior suggests that other interactions, such as van der Waals forces and hydrophobic effects, may play a major role in promoting adsorption under acidic conditions [42,51]. In contrast, at pH values above 3.7, RhB transitions to a zwitterionic form and tends to aggregate into larger macromolecular structures [52], which decreases its availability for adsorption.

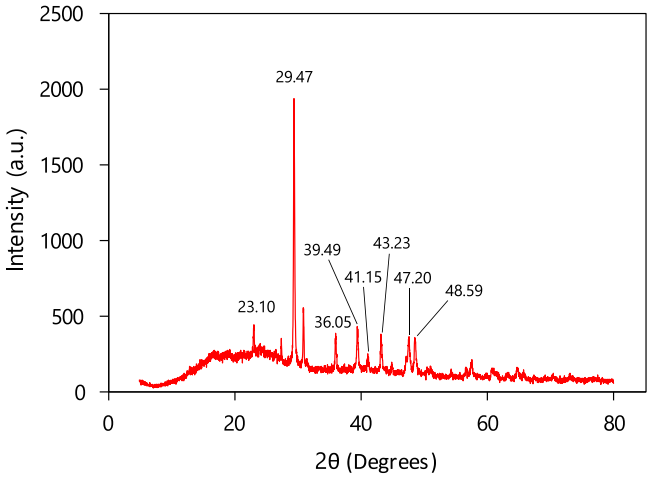


Fig. 3. XRD pattern of PVC-MPs showing crystalline peaks.

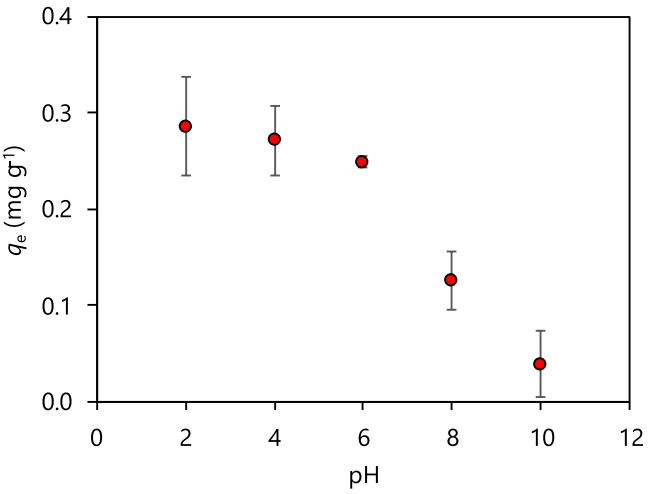


Fig. 4. Effect of solution pH on RhB adsorption capacity of PVC-MPs.

3.3. Effect of MPs dose on adsorption

The adsorption behavior of RhB onto PVC-MPs as a function of microplastic dosage is presented in Fig. 5. The experiments were conducted using an initial RhB concentration of 20 mg L^{-1}, which lies within the range commonly reported for textile dye effluents (10–250 mg L^{-1}) [53]. As the dosage increased from 50 to 100 mg, the adsorption capacity rose from 0.23 to 0.36 mg g^{-1}. However, further increases in dosage to 200, 300, and 400 mg did not result in significant variation, with the adsorption capacity stabilizing around 0.33 mg g^{-1}. This behavior contrasts with the trend commonly reported in the literature, in which adsorption capacity typically decreases with increasing adsorbent dosage [1,33]. Such decreases are often attributed to an excess of available adsorption sites relative to the amount of adsorbate, leading to site underutilization and reduced adsorption efficiency. In the

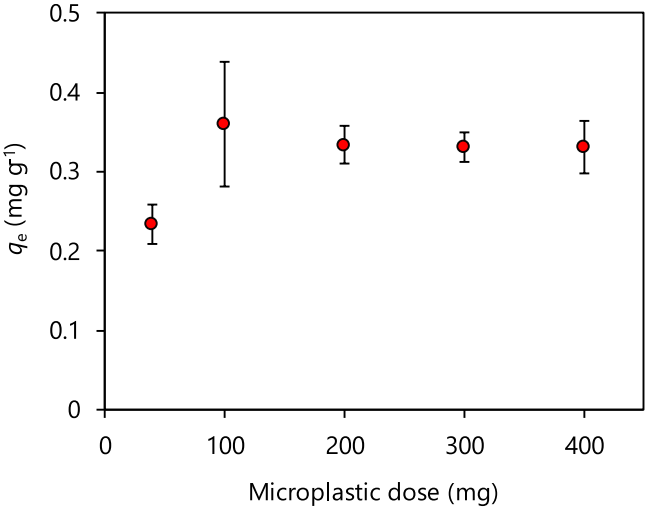


Fig. 5. Effect of PVC-MP dosage on RhB adsorption.

present study, the observed stabilization, rather than a decline, suggests the influence of additional factors. One possibility is a strong affinity between RhB molecules and the PVC-MP surface, which may sustain adsorption capacity even at higher dosages. Furthermore, particle aggregation, which can limit surface area availability, may not have been pronounced enough to negatively affect adsorption performance under the tested conditions.

3.4. Adsorption kinetics

Fig. 6 illustrates the kinetic behavior of RhB adsorption on PVC-MPs. The adsorption capacity increased with rising initial dye concentrations, which can be attributed to the higher probability of collisions between dye molecules and active sites on the polymer surface [34]. Most of the uptake occurred rapidly within the first 1–3 h, after which the adsorption rate slowed considerably, indicating the progressive attainment of equilibrium (Fig. 6a).

Table 1 presents the kinetic constants obtained from the PFO and PSO models, along with the corresponding R^2 and RMSE. Both models described the data reasonably well, however, the PFO model consistently produced q_e values that were closer to the experimental measurements across all concentrations, in addition to slightly higher R^2 values at elevated dye levels. Conversely, the PSO model showed a tendency to overpredict q_e. This closer alignment between the experimental and PFO-predicted capacities indicates that the PFO model provides the most reliable description of the kinetic process under the tested conditions. Since this model is typically associated with physisorption, its superior performance reinforces the conclusion that the adsorption of RhB onto PVC-MPs is dominated by weak physical interactions rather than chemisorption [54].

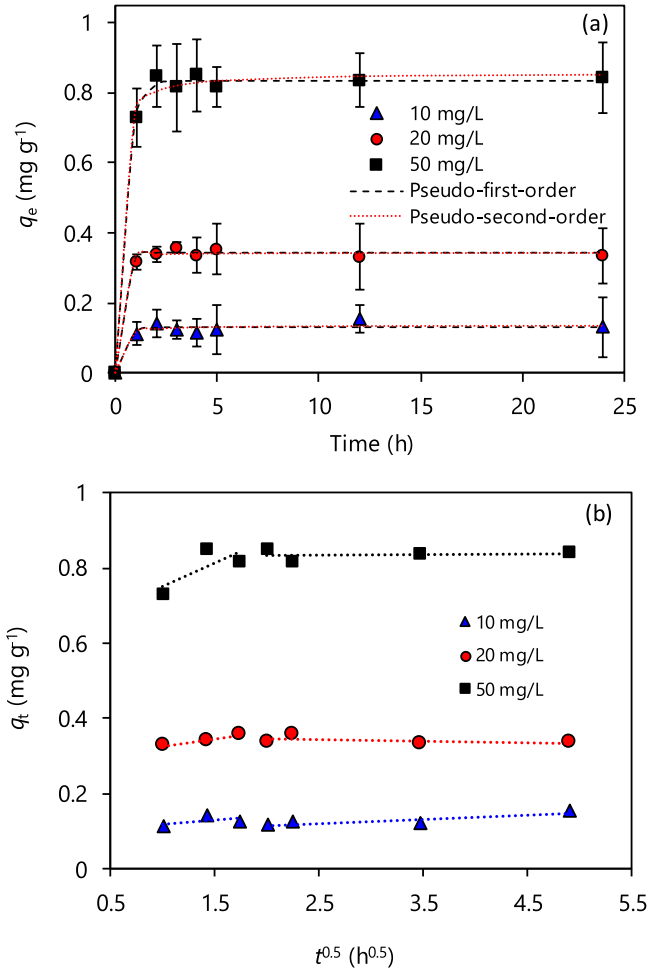


Fig. 6. Kinetic models for RhB adsorption onto PVC-MPs: (a) pseudo-first-order (PFO) and pseudo-second-order (PSO) models; (b) intraparticle diffusion model.

Table 1
Parameters of kinetic models for RhB adsorption onto PVC-MPs (experimental conditions: natural pH 5.5, 25 °C, PVC-MP dosage 100 mg, solution volume 40 mL, agitation 180 rpm).

Parameter	RhB concentration (mg L^{-1})		
	10	20	50
Experimental data (mg g^{-1})	0.132	0.334	0.843
PFO model			
q_e (mg g^{-1})	0.132	0.342	0.836
k_1 (h^{-1})	2.021	2.596	2.120
R^2	0.936	0.994	0.997
RMSE	0.013	0.010	0.016
PSO model			
q_e (mg g^{-1})	0.138	0.346	0.856
k_2 (mg g^{-1} h^{-1})	36.330	48.372	87.201
R^2	0.938	0.991	0.994
RMSE	0.013	0.012	0.025
Intraparticle diffusion model			
Step 1			
K_{id} (mg g^{-1} min$^{-0.5}$)	0.021	0.041	0.125
C (mg g^{-1})	0.098	0.284	0.626
R^2	0.249	0.969	0.571
RMSE	0.018	0.004	0.056
Step 2			
K_{id} (mg g^{-1} min$^{-0.5}$)	0.011	0.004	0.003
C (mg g^{-1})	0.093	0.352	0.828
R^2	0.755	0.294	0.055
RMSE	0.011	0.011	0.017

To clarify the mechanisms controlling the adsorption rate of RhB onto PVC-MPs, the intraparticle diffusion model was employed. As shown in Fig. 6b, the adsorption process followed a two-step profile: a rapid initial phase attributed to surface adsorption, followed by a slower phase associated with intraparticle diffusion. This two-phase behavior became more evident at higher RhB concentrations (e.g., 50 mg L^{-1}), likely because the greater abundance of dye molecules enhances the shift from surface binding to restricted internal diffusion. The presence of positive intercepts in the plots indicates that intraparticle diffusion was not the only factor limiting the rate of adsorption, implying the additional influence of boundary layer resistance [55]. Considering the minimal porosity revealed by the BJH analysis (0.0010 cm^3 g^{-1}), the slower kinetic phase is unlikely to result from diffusion through a well-developed pore network. Instead, it more plausibly reflects the limited penetration of RhB molecules into structural imperfections, amorphous domains, or microfissures within the compact polymer matrix of PVC-MPs.

3.5. Adsorption isotherms

Analysis of adsorption isotherms provides insights into the nature of the interaction between adsorbent and adsorbate, as well as the capacity and efficiency of the process under different experimental conditions. The isotherm fitting curves for RhB uptake by PVC-MPs, based on the Langmuir, Freundlich, Temkin, and D–R models, are shown in Fig. 7, and the estimated parameters are listed in Table 2.

Among the tested models, Temkin and D–R provided the best fits, with R^2 values of 0.967 and 0.968, respectively, and the lowest RMSE values. This superior performance reflects key features of the adsorption system. The Temkin model assumes a linear decrease in the heat of adsorption with increasing surface coverage [41], which is consistent with the heterogeneous energy distribution expected on the irregular PVC-MPs surface. This behavior suggests that adsorption sites are not energetically uniform, and that adsorbate–adsorbate interactions become relevant as the surface becomes progressively occupied [54]. Additionally, the Temkin heat constant (b_T = 5783.83 J mol^{-1})

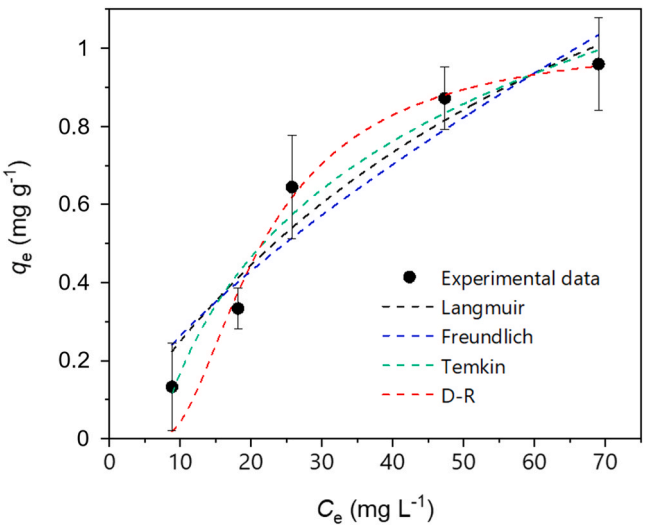


Fig. 7. Adsorption isotherms for RhB onto PVC-MPs fitted with the Langmuir, Freundlich, Temkin, and Dubinin–Radushkevich (D–R) models.

Table 2
Calculated isotherm parameters for RhB adsorption onto PVC-MPs based on Langmuir, Freundlich, Temkin, and D-R models (experimental conditions: natural pH 5.5, 25 °C, PVC-MP dosage 100 mg, solution volume 40 mL, agitation 180 rpm, initial dye concentration 10–75 mg L^{-1}).

Model	Parameter
Langmuir	
q_{max} (mg g^{-1})	2.088
K_L (L mg^{-1})	0.0136
R^2	0.938
RMSE	0.1015
Freundlich	
K_F (mg g^{-1}) (mg L^{-1})$^{-1/n}$	0.0513
n	1.4100
R^2	0.908
RMSE	0.1229
Temkin	
A_T (L g^{-1})	0.1480
b_T (J mol^{-1})	5783.83
R^2	0.967
RMSE	0.0736
D-R	
q_{max} (mg g^{-1})	1.027
K_{DR} (mol^2 J^{-2})	5.69 × 10^{-5}
E (kJ mol^{-1})	0.0937
R^2	0.968
RMSE	0.0722

indicates an exothermic process [56].

The D–R model, often applied to gain insight into the adsorption mechanism, yielded complementary information. The calculated mean free energy of adsorption (E = 0.0937 kJ mol^{-1}) is far below 8 kJ mol^{-1} , indicating that the process is dominated by weak physical interactions such as van der Waals forces and hydrophobic effects [57], in line with the interpretation from the PFO kinetic model.

Although the Langmuir model produced a slightly lower R^2 value (0.938), it still allowed a reliable estimation of the maximum adsorption capacity (q_{max} = 2.088 mg g^{-1}). Studies in the literature have reported a wide range of q_{max} values for RhB adsorption onto different types of microplastics, reflecting the strong influence of polymer composition and surface properties. For example, Du et al. [50] reported q_{max} values of 4.598 mg g^{-1} for PVC, 2.482 mg g^{-1} for polystyrene (PS), and 1.788 mg g^{-1} for polyethylene terephthalate (PET), indicating that PVC generally shows higher affinity for RhB than PS and PET. Likewise, Li et al. [58] observed q_{max} values of 3.844 mg g^{-1} for pristine polylactic acid microplastic and 3.389 mg g^{-1} for pristine polyamide 66 microplastic, which increased to 45.224 and 4.661 mg g^{-1}, respectively, after ultraviolet aging. This substantial enhancement upon aging was attributed to surface oxidation and increased roughness, which introduce additional adsorption sites. A broader comparison of q_{max} values reported for different combinations of microplastics and dyes is provided in Table S1.

In contrast, the Freundlich model exhibited the weakest statistical adjustment (R^2 = 0.908), indicating a less accurate description of the adsorption equilibrium for this system. Nonetheless, the Freundlich constant (n = 1.41) confirmed that the conditions remained favorable for adsorption [59].

3.6. Performance of the ANN and SVR models

The ANN models were optimized using the backpropagation algorithm, in which weights and biases are iteratively updated to reduce the error between predicted and experimental outputs. Training was performed for up to 1000 cycles (default), with the learning rate automatically adjusted by the software. Early stopping was applied to avoid overfitting. Table 3 summarizes the five network architectures tested, highlighting the activation functions used in the hidden and output layers. All configurations demonstrated excellent predictive accuracy, with R^2 values above 0.99 for the test dataset. The best results were obtained with the 4–9–1 architecture, which employed four input neurons, nine neurons in a single hidden layer, and one output neuron. This network used the hyperbolic tangent (tanh) as the hidden-layer activation function and an exponential function in the output layer. Under this configuration, the model achieved the highest R^2 (0.999) and the lowest RMSE (0.0142) for the test set, confirming its robustness and ability to generalize well to unseen data.

SVR models were also developed, with hyperparameters C (penalty factor), ε (epsilon-insensitive loss), and γ (kernel coefficient) optimized through a trial-and-error approach. Table 4 summarizes the selected hyperparameters and corresponding performance metrics. The best SVR configuration achieved an R^2 of 0.992 and an RMSE of 0.0327 on the test data, demonstrating strong predictive capability for adsorption behavior.

Both ANN and SVR models successfully captured the complex, nonlinear relationships among the process variables governing RhB adsorption onto PVC-MPs (Fig. 8). While the ANN model provided slightly better results than SVR in terms of R^2 and RMSE on the test dataset, the two approaches showed strong generalization ability and proved to be reliable strategies for modeling adsorption behavior.

Although both ANN and SVR exhibit strong predictive capacity, they also have inherent limitations. ANN models, for instance, are prone to overfitting when applied to small datasets and demand careful adjustment of network structure and hyperparameters [60]. In contrast, SVR can become computationally demanding for large datasets and its performance is strongly influenced by the selection of kernel functions and parameter settings [44]. Therefore, proper model configuration and validation are essential to ensure accurate and reliable predictions in adsorption studies.

Even with these constraints, numerous studies have confirmed the usefulness of ANN and SVR for adsorption modeling. For example, Eroğlu et al. [61] applied ANN to model RhB adsorption onto biochar from pine nut shells, achieving an R^2 of 0.983 on the test set. Similarly, SVR models have been employed successfully for various adsorbents, such as the work by Usman et al. [62] with activated pomegranate peel and Aftab et al. [63] with black cardamom-derived activated carbon. Collectively, these findings reinforce the applicability of machine learning models such as ANN and SVR as reliable predictive tools in adsorption studies.

Table 3
ANN model architectures for RhB adsorption onto PVC-MPs.

ANN model architecture	R^2 (Training)	R^2 (Test)	RMSE (Training)	RMSE (Test)	Hidden activation	Output activation
4–9–1	**0.990**	**0.999**	**0.0275**	**0.0142**	**Tanh**	**Exponential**
4–8–1	0.992	0.997	0.0245	0.0191	Tanh	Identity
4–20–1	0.990	0.998	0.0269	0.0199	Tanh	Exponential
4–5–1	0.961	0.995	0.0548	0.0225	Tanh	Exponential
4–14–1	0.962	0.996	0.0534	0.0255	Logistic	Logistic

Table 4
Optimized hyperparameters and performance for the SVR model.

Model	C	γ	ε	No. of support vectors	R^2 (Training)	R^2 (Test)	RMSE (Training)	RMSE (Test)
SVR	10	1	0.02	22	0.984	0.992	0.0354	0.0327

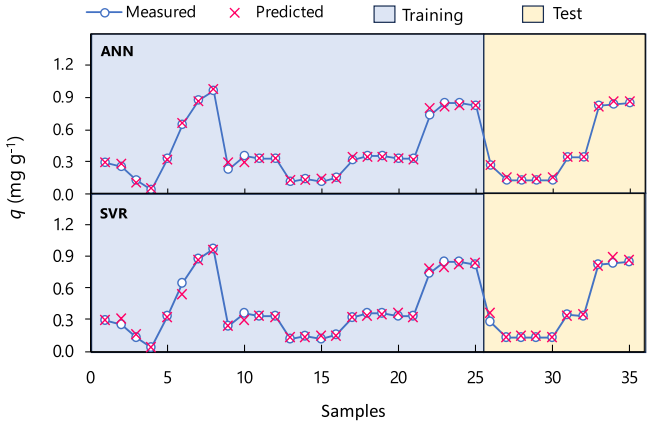


Fig. 8. Predictive performance of ANN and SVR models for RhB adsorption onto PVC-MPs.

3.7. Probable adsorption mechanism

Clarifying the mechanism of RhB adsorption onto PVC-MPs is important for interpreting the trends observed in this work. The process appears to be predominantly governed by weak physicochemical interactions rather than strong chemical bonding. FTIR analysis revealed no evidence of new bond formation between the PVC-MPs and RhB, supporting the predominance of physisorption. Instead, slight changes in band intensity suggest the contribution of non-covalent interactions, particularly hydrogen and halogen bonding, likely involving surface functionalities of PVC and the aromatic rings of RhB [41,50].

At pH values below the point of zero charge, both the PVC surface and RhB molecules carry positive charges, which would normally lead to electrostatic repulsion. Despite this, appreciable adsorption was observed under acidic conditions, indicating that alternative mechanisms exerted greater influence. In particular, π–π stacking, van der Waals forces, and hydrophobic interactions are likely to dominate the adsorption process in this pH range [50,51].

Further insight into the adsorption mechanism was obtained from isotherm modeling. The Temkin model indicated a progressive decrease in adsorption energy with increasing surface coverage, suggesting energetic heterogeneity on the PVC-MPs surface and exothermic interactions. The D–R model also supported the dominance of physisorption, as indicated by the very low mean free energy values, in agreement with both the kinetic analysis and FTIR observations. Overall, RhB adsorption onto PVC-MPs appears to result from a combination of surface adsorption and limited diffusion-driven processes, mediated by multiple weak, non-specific interactions.

4. Conclusion

This study demonstrated that PVC microplastics can act as effective vectors for the transport of synthetic dyes in aquatic environments. Despite their compact structure and low surface area (0.1713 $m^2\ g^{-1}$), PVC-MPs exhibited a measurable adsorption capacity for Rhodamine B, reaching a maximum of 2.09 mg g^{-1} under acidic conditions. Kinetic analysis revealed that the pseudo-first-order model best described the adsorption process ($R^2 > 0.98$), indicating the predominance of physisorption. Equilibrium data were best fitted by the Temkin ($R^2 = 0.967$) and Dubinin–Radushkevich ($R^2 = 0.968$) models, with a very low mean adsorption energy (E = 0.0937 kJ mol^{-1}), confirming weak interactions such as hydrophobic effects, van der Waals forces, and hydrogen and halogen bonding. Artificial intelligence models exhibited excellent predictive performance for RhB adsorption capacity. The best ANN configuration achieved $R^2 = 0.999$ and RMSE = 0.0142, while the optimized SVR model reached $R^2 = 0.992$ and RMSE = 0.0327 on the test set. These results confirm the robustness of AI-based approaches for capturing complex nonlinear relationships among environmental variables and predicting contaminant–microplastic interactions with high accuracy. The environmental implications of these findings are considerable. Even moderate adsorption capacities can increase the persistence and mobility of synthetic dyes, raising concerns about ecological toxicity, bioaccumulation, and human exposure through contaminated water and biota. Further research should address field validation, long-term behavior, and risk assessment of dye–microplastic complexes to better support environmental risk evaluations and mitigation strategies.

CRediT authorship contribution statement

Eduardo Beraldo de Morais: Writing – review & editing, Writing – original draft, Visualization, Validation, Project administration, Investigation, Formal analysis, Conceptualization. **Danila Soares Caixeta:** Writing – review & editing, Writing – original draft, Visualization, Conceptualization. **Vinícius Reis Cargnelutti:** Investigation, Formal analysis, Data curation, Conceptualization. **Paulo Renato Matos Lopes:** Writing – review & editing, Writing – original draft, Visualization, Conceptualization. **Leonardo Gomes de Vasconcelos:** Writing – review & editing, Writing – original draft, Visualization, Conceptualization. **Rodrigo Esaú Vassoler e Silva:** Methodology, Investigation, Formal analysis, Data curation. **Amanda Alcaide Francisco Fukumoto:** Writing – review & editing, Writing – original draft, Validation, Methodology. **Rossean Golin:** Methodology, Investigation, Formal analysis, Data curation. **Frederico Carlos Martins de Menezes Filho:** Writing – review & editing, Writing – original draft, Visualization, Conceptualization. **Ibraim Fantin da Cruz:** Writing – review & editing, Writing – original draft, Visualization, Conceptualization.

Declaration of Generative AI and AI-assisted technologies in the writing process

During the preparation of this work, the authors used ChatGPT (version 4) to assist in correcting and improving the writing of this manuscript. The tool was used to enhance the clarity, flow, and overall readability of the text. After using this tool, the authors reviewed and edited the content as needed and take full responsibility for the content of the publication.

Declaration of Competing Interest

The authors declare that they have no known competing financial interests or personal relationships that could have appeared to influence the work reported in this paper.

Appendix A. Supporting information

Supplementary data associated with this article can be found in the online version at doi:10.1016/j.dwt.2025.101558.

Data availability

No data was used for the research described in the article.

References

[1] Anastopoulos I, Pashalidis I, Kayan B, Kalderis D. Microplastics as carriers of hydrophilic pollutants in an aqueous environment. J Mol Liq 2022;350. https://doi.org/10.1016/j.molliq.2021.118182.

[2] Chen Z, Fang J, Wei W, Ngo HH, Guo W, Ni BJ. Emerging adsorbents for micro/nanoplastics removal from contaminated water: advances and perspectives. J Clean Prod 2022;371. https://doi.org/10.1016/j.jclepro.2022.133676.

[3] Osman AI, Hosny M, Eltaweil AS, Omar S, Elgarahy AM, Farghali M, et al. Microplastic sources, formation, toxicity and remediation: a review. Environ Chem Lett 2023;21:2129–69. https://doi.org/10.1007/s10311-023-01593-3.

[4] Xiong F, Liu J, Xu K, Huang J, Wang D, Li F, et al. Microplastics induce neurotoxicity in aquatic animals at environmentally realistic concentrations: a meta-analysis. Environ Pollut 2023;318. https://doi.org/10.1016/j.envpol.2022.120939.

[5] Zhuo T, Chai B, yi You X. Modeling the spatiotemporal distribution, bioaccumulation, and ecological risk assessment of microplastics in aquatic ecosystems: a review. Aquat Toxicol 2025;279. https://doi.org/10.1016/j.aquatox.2024.107210.

[6] Li Y, Ling W, Hou C, Yang J, Xing Y, Lu Q, et al. Global distribution characteristics and ecological risk assessment of microplastics in aquatic organisms based on meta-analysis. J Hazard Mater 2025;491. https://doi.org/10.1016/j.jhazmat.2025.137977.

[7] Kida M, Ziembowicz S, Pochwat K, Koszelnik P, Piekutin J. Pollution of the aquatic environment by plasticizers leached from microplastics originating from linear sewage systems. Desalin Water Treat 2025;322. https://doi.org/10.1016/j.dwt.2025.101122.

[8] Ziembowicz S, Kida M. The abundance, characteristics and ecological risk assessment of microplastics in rainwater – preliminary study. Desalin Water Treat 2025;322. https://doi.org/10.1016/j.dwt.2025.101111.

[9] Esmaeili Nasrabadi A, Zahmatkesh Anbarani M, Bonyadi Z. Investigating the efficiency of oak powder as a new natural coagulant for eliminating polystyrene microplastics from aqueous solutions. Sci Rep 2023;13. https://doi.org/10.1038/s41598-023-47849-4.

[10] Esmaeili Nasrabadi A, Bonyadi Z. Adsorption of crystal violet on polystyrene microplastics in aqueous: optimization, modeling, and assessment of isotherms and kinetics. Appl Water Sci 2025;15. https://doi.org/10.1007/s13201-025-02418-0.

[11] Zhang J, Ma C, Zhang J, Li Z, Xu Z, Zhang S, et al. Nanoplastics drive the charge-specific decline of aquatic insect (*Chironomus kiinensis*) emergence through inducing oxidative damage and perturbing the endocrine system. Environ Sci Technol 2025. https://doi.org/10.1021/acs.est.5c04923.

[12] Atugoda T, Vithanage M, Wijesekara H, Bolan N, Sarmah AK, Bank MS, et al. Interactions between microplastics, pharmaceuticals and personal care products: implications for vector transport. Environ Int 2021;149. https://doi.org/10.1016/j.envint.2020.106367.

[13] Kinigopoulou V, Pashalidis I, Kalderis D, Anastopoulos I. Microplastics as carriers of inorganic and organic contaminants in the environment: a review of recent progress. J Mol Liq 2022;350. https://doi.org/10.1016/j.molliq.2022.118580.

[14] Joo SH, Liang Y, Kim M, Byun J, Choi H. Microplastics with adsorbed contaminants: mechanisms and treatment. Environ Chall 2021;3. https://doi.org/10.1016/j.envc.2021.100042.

[15] Esmaeili Nasrabadi A, Bonyadi Z. Evaluation of the rate of *Chlorella vulgaris* biofilm on polyvinyl chloride microplastics in aqueous solutions. Results Eng 2025;26. https://doi.org/10.1016/j.rineng.2025.105189.

[16] Song X, Zhuang W, Cui H, Liu M, Gao T, Li A, et al. Interactions of microplastics with organic, inorganic and bio-pollutants and the ecotoxicological effects on terrestrial and aquatic organisms. Sci Total Environ 2022;838. https://doi.org/10.1016/j.scitotenv.2022.156068.

[17] Wang K, Wang K, Chen Y, Liang S, Guo C, Wang W, et al. Adsorption–desorption behavior of malachite green by potassium permanganate pre-oxidation polyvinyl chloride microplastics. Environ Technol Innov 2023;30. https://doi.org/10.1016/j.eti.2023.103138.

[18] Ali AAM, Anuar ST, Azmi AA, Yusof KMKK, Khalik WMAWM, Ibrahim YS. Microplastics as the vector for the attachment of polychlorinated biphenyls: A case study of urbanized Langat River, Malaysia. Mar Pollut Bull 2025;220. https://doi.org/10.1016/j.marpolbul.2025.118382.

[19] Zeng Z, Jia B, Liu X, Chen L, Zhang P, Qing T, et al. Adsorption behavior of triazine pesticides on polystyrene microplastics aging with different processes in natural environment. Environ Pollut 2024;356. https://doi.org/10.1016/j.envpol.2024.124319.

[20] Frescura LM, de Menezes BB, Junior RAF, Mortari SR, de Moraes Bastos AF, da Rosa MB. Polycyclic aromatic hydrocarbon derivatives onto polar microplastics of polyurethane: equilibrium, thermodynamics, and kinetics of monolayer-multilayer adsorption. Environ Sci Pollut Res 2024;31:55158–68. https://doi.org/10.1007/s11356-024-34848-9.

[21] Cai N, Xu H, Yu Z, Xie Y. Pollution characterization, adsorption, and SERS-based detection of enrofloxacin adsorbed on microplastics in aquaculture water. Environ Res 2025;285. https://doi.org/10.1016/j.envres.2025.122594.

[22] Beljin J, Kragulj Isakovski M, Simetić T, Đukanović N, Molnar Jazić J, Maletić S, et al. Exploring the adsorption behavior of organic UV filter on carbon-based materials as potential carriers of organic contaminants in the aquatic environment. Appl Sci 2024;14. https://doi.org/10.3390/app14209424.

[23] Jiang H, Hu H. Sustainable synergistic adsorption of tetracycline in water by biochar and microplastics: exploration of the mechanism of DFT. J Water Process Eng 2024;66. https://doi.org/10.1016/j.jwpe.2024.105998.

[24] Yari M, Bonyadi Z, Najafpoor A, Barikbin B. Polyethylene microplastics as adsorbent of diazinon in aqueous environments: optimization, and modeling, isotherm, kinetics, and thermodynamic studies. Appl Water Sci 2024;14. https://doi.org/10.1007/s13201-024-02213-3.

[25] Barari F, Eydi Gabrabad M, Bonyadi Z, Ramavandi B. Advances in metal-organic frameworks for microplastic removal from aquatic environments: mechanisms and performance insights. Results Chem 2025;14. https://doi.org/10.1016/j.rechem.2025.102132.

[26] Khoshmanesh M, Sanati AM, Shahcheragh S, Farjadfard S, Bonyadi Z, Ramavandi B. Recent advances in dyes uptake by microplastics in aquatic environments: influencing factors and ecotoxicological behaviors. Arab J Chem 2024;17. https://doi.org/10.1016/j.arabjc.2024.105737.

[27] Kaci MM, Nasrallah N, Djaballah AM, Akkari I, Belabed C, Soukeur A, et al. Insights into the optical and electrochemical features of CuAl2O4 nanoparticles and it use for methyl violet oxidation under sunlight exposure. Opt Mater 2022;126. https://doi.org/10.1016/j.optmat.2022.112198.

[28] Soukeur A, Kaci MM, Omeiri S, Bellal B, Amara M, Trari M. Photocatalytic degradation of bromothymol blue over $MgFe_2O_4$ under sunlight exposure. Opt Mater (Amst) 2023;142. https://doi.org/10.1016/j.optmat.2023.114108.

[29] Shahnawaz Khan M, Khalid M, Shahid M. What triggers dye adsorption by metal organic frameworks? The current perspectives. Mater Adv 2020;1:1575–601. https://doi.org/10.1039/d0ma00291g.

[30] Khan MS, Li Y, Li DS, Qiu J, Xu X, Yang HY. A review of metal-organic framework (MOF) materials as an effective photocatalyst for degradation of organic pollutants. Nanoscale Adv 2023;5:6318–48. https://doi.org/10.1039/d3na00627a.

[31] Kumari S, Singh R, Jahangeer J, Garg MC. Innovative strategies for dye removal from textile wastewater: A comprehensive review of treatment approaches and challenges. Water Air Soil Pollut 2024;235. https://doi.org/10.1007/s11270-024-07532-4.

[32] La Maestra S, Benvenuti M, Gaggero L, Damonte G, Salis A, Alberti S, et al. Environmental microplastics as vectors of non-polar organic pollutants in drinking water. Environments 2025;12. https://doi.org/10.3390/environments12030081.

[33] Bahrami M, Amiri MJ, Rajabi S, Mahmoudi M. The removal of methylene blue from aqueous solutions by polyethylene microplastics: modeling batch adsorption using random forest regression. Alex Eng J 2024;95:101–13. https://doi.org/10.1016/j.aej.2024.03.100.

[34] Santos TPM dos, Dias BM, Sousa HM, de Menezes Filho FCM, Fukumoto AAF, da Cruz IF, et al. Adsorption of rhodamine B onto cotton straw-derived biochar: kinetic, equilibrium, thermodynamics, and predictive studies using artificial intelligence. Int J Phytoremediat 2025. https://doi.org/10.1080/15226514.2025.2527937.

[35] Kaya N, Yıldız Uzun Z, Altuncan C, Uzun H. Adsorption of Congo red from aqueous solution onto KOH-activated biochar produced via pyrolysis of pine cone and modeling of the process using artificial neural network. Biomass Convers Biorefin 2022;12:5293–315. https://doi.org/10.1007/s13399-021-01856-5.

[36] Kumar GVSRP, Pydiraju YB, Lokesh GV, Likith UVS. Removal of rhodamine B using three adsorbents: isothermal, kinetic, and ANN modeling studies. Water Conserv Sci Eng 2023;8. https://doi.org/10.1007/s41101-023-00191-2.

[37] Nascimento MX, dos Santos BAP, Nassarden MMS, dos K, Nogueira S, da RG, et al. Artificial neural network-based modeling of Malachite green adsorption onto baru fruit endocarp: insights into equilibrium, kinetic, and thermodynamic behavior. Int

J Phytoremediat 2024;26:1749–63. https://doi.org/10.1080/15226514.2024.2354411.
[38] Baum P, Kuch B, Dittmer U. Adsorption of metals to particles in urban stormwater runoff—does size really matter? Water 2021;13:1–21. https://doi.org/10.3390/w13030309.
[39] Khoshmanesh M, Sanati AM, Ramavandi B. Influence of cephalexin on cadmium adsorption onto microplastic particles in water: Human health risk evaluation. Heliyon 2024;10. https://doi.org/10.1016/j.heliyon.2024.e37775.
[40] Akkari I, Spessato L, Graba Z, Bezzi N, Kaci MM. A sustainably produced hydrochar from pomegranate peels for the purification of textile contaminants in an aqueous medium. Sustain Chem Pharm 2023;31. https://doi.org/10.1016/j.scp.2022.100924.
[41] Bao ZZ, Chen ZF, Zhong Y, Wang G, Qi Z, Cai Z. Adsorption of phenanthrene and its monohydroxy derivatives on polyvinyl chloride microplastics in aqueous solution: model fitting and mechanism analysis. Sci Total Environ 2021;764. https://doi.org/10.1016/j.scitotenv.2020.142889.
[42] Zahmatkesh Anbarani M, Najafpoor A, Barikbin B, Bonyadi Z. Adsorption of tetracycline on polyvinyl chloride microplastics in aqueous environments. Sci Rep 2023;13. https://doi.org/10.1038/s41598-023-44288-z.
[43] Astray G, Soria-Lopez A, Barreiro E, Mejuto JC, Cid-Samamed A. Machine learning to predict the adsorption capacity of microplastics. Nanomaterials 2023;13. https://doi.org/10.3390/nano13061061.
[44] Herceg S, Ujević Andrijić Ž, Bolf N. Development of soft sensors for isomerization process based on support vector machine regression and dynamic polynomial models. Chem Eng Res Des 2019;149:95–103. https://doi.org/10.1016/j.cherd.2019.06.034.
[45] Canayaz M, Aldemir A, Kul AR. Application of machine learning methods to removal percentage prediction for Malachite green adsorption on kaolinite. Desalin Water Treat 2022;247:258–71. https://doi.org/10.5004/dwt.2022.28036.
[46] Abedpour H, Moghaddas J, Sori A, Alizadeh R. Experimental study and machine learning simulation of Pb (II) separation from aqueous solutions via a nanocomposite adsorbent. J Taiwan Inst Chem Eng 2023;147. https://doi.org/10.1016/j.jtice.2023.104923.
[47] Meng J, Xu B, Liu F, Li W, Sy N, Zhou X, et al. Effects of chemical and natural ageing on the release of potentially toxic metal additives in commercial PVC microplastics. Chemosphere 2021;283. https://doi.org/10.1016/j.chemosphere.2021.131274.
[48] Tubić A, Vujić M, Gvoić V, Agbaba J, Vasiljević S, Cveticanin L, et al. Sorption potential of microplastics for azo- and phthalocyanine printing dyes. Dyes Pigments 2023;209. https://doi.org/10.1016/j.dyepig.2022.110884.
[49] Zhong Y, Ding Q, Huang Z, Xiao X, Han X, Su Y, et al. Influence of ultraviolet-aging and adsorbed pollutants on toxicological effects of polyvinyl chloride microplastics to zebrafish. Environ Pollut 2023;316. https://doi.org/10.1016/j.envpol.2022.120617.
[50] Du H, Zhang Y, Jiang H, Wang H. Adsorption of rhodamine B on polyvinyl chloride, polystyrene, and polyethylene terephthalate microplastics in aqueous environments. Environ Technol Innov 2022;27. https://doi.org/10.1016/j.eti.2022.102495.
[51] Liang Y, Ying C, Zhu J, Zhou Q, Sun K, Tian Y, et al. Effects of salinity, pH, and Cu (II) on the adsorption behaviors of tetracycline onto polyvinyl chloride microplastics: A site energy distribution analysis. Water 2023;15. https://doi.org/10.3390/w15101925.
[52] Shaikh WA, Islam RU, Chakraborty S. Stable silver nanoparticle doped mesoporous biochar-based nanocomposite for efficient removal of toxic dyes. J Environ Chem Eng 2021;9. https://doi.org/10.1016/j.jece.2020.104982.
[53] da Rosa ALD, Carissimi E, Dotto GL, Sander H, Feris LA. Biosorption of rhodamine B dye from dyeing stones effluents using the green microalgae *Chlorella pyrenoidosa*. J Clean Prod 2018;198:1302–10. https://doi.org/10.1016/j.jclepro.2018.07.128.
[54] Hao L, Ma H, Xing B. Surface characteristics and adsorption properties of polypropylene microplastics by ultraviolet irradiation and natural aging. Sci Total Environ 2024;944. https://doi.org/10.1016/j.scitotenv.2024.173962.
[55] Atmani F, Kaci MM, Akkari I, Yeddou-Mezenner N, Bensaadi-Ouznadji Z, Balamane-Zizi O, et al. Adsorption ability of sugar scum as industrial waste for crystal violet elimination: experimental and advanced statistical physics modeling. Surf Interfaces 2024;54. https://doi.org/10.1016/j.surfin.2024.105166.
[56] Zeng S, Choi YK, Kan E. Iron-activated bermudagrass-derived biochar for adsorption of aqueous sulfamethoxazole: effects of iron impregnation ratio on biochar properties, adsorption, and regeneration. Sci Total Environ 2021;750. https://doi.org/10.1016/j.scitotenv.2020.141691.
[57] Atmani F, Kaci MM, Yeddou-Mezenner N, Soukeur A, Akkari I, Navio JA. Insights into the physicochemical properties of Sugar Scum as a sustainable biosorbent derived from sugar refinery waste for efficient cationic dye removal. Biomass Convers Biorefin 2024;14:4843–57. https://doi.org/10.1007/s13399-022-02646-3.
[58] Li J, Wang K, Wang K, Liang S, Guo C, Hassan A, et al. Adsorption behavior of Methylene Blue and Rhodamine B on microplastics before and after ultraviolet irradiation. Colloids Surf A Physicochem Eng Asp 2024;699. https://doi.org/10.1016/j.colsurfa.2024.134671.
[59] Kaci MM, Akkari I, Pazos M, Atmani F, Akkari H. Recent trends in remediating Basic Red 46 dye as a persistent pollutant from water bodies using promising adsorbents: a review. Clean Technol Environ Policy 2024. https://doi.org/10.1007/s10098-024-03026-3.
[60] Chu J, Liu X, Zhang Z, Zhang Y, He M. A novel method overcomeing overfitting of artificial neural network for accurate prediction: application on thermophysical property of natural gas. Case Stud Therm Eng 2021;28. https://doi.org/10.1016/j.csite.2021.101406.
[61] Atalay Eroğlu H, Kadıoğlu EN, Akbal F. High-efficiency removal of Rhodamine B using modified biochar from agricultural waste pine nut shell: investigation of kinetics, isotherms, and artificial neural network modeling. Biomass Convers Biorefin 2024. https://doi.org/10.1007/s13399-024-06045-8.
[62] Usman MA, Aftab RA, Zaidi S, Adnan SM, Rao RAK. Adsorption of aniline blue dye on activated pomegranate peel: equilibrium, kinetics, thermodynamics and support vector regression modelling. Int J Environ Sci Technol 2022;19:8351–68. https://doi.org/10.1007/s13762-021-03571-0.
[63] Ahmad Aftab R, Zaidi S, Aslam Parwaz Khan A, Arish Usman M, Khan AY, Tariq Saeed Chani M, et al. Removal of Congo red from water by adsorption onto activated carbon derived from waste black cardamom peels and machine learning modeling. Alex Eng J 2023;71:355–69. https://doi.org/10.1016/j.aej.2023.03.055.